Available online at www.sciencedirect.com
SCIENCE DIRECT®
Journal of Catalysis 221 (2004) 523–531
JOURNAL OF CATALYSIS
www.elsevier.com/locate/jcat

Dielectric heating effects on the activity and SO_2 resistance of $La_{0.8}Ce_{0.2}MnO_3$ perovskite for methane oxidation

Y. Zhang-Steenwinkel, H.L. Castricum, J. Beckers, E. Eiser, and A. Bliek *

Department of Chemical Engineering, University of Amsterdam, Nieuwe Achtergracht 166, 1018 WV Amsterdam, The Netherlands

Received 6 May 2003; revised 14 August 2003; accepted 8 September 2003

Abstract

The catalytic activity in CH_4 oxidation over a $La_{0.8}Ce_{0.2}MnO_3$ perovskite as a model reaction is investigated under dielectric and conventional heating conditions. As these materials are both microwave sensitive and catalytically active, they may be applied as coating material for ceramic soot filters for the reduction of soot emission from diesel engines. Dielectric heating is shown to result in a much higher CH_4 conversion and a higher resistance to SO_2 poisoning. We propose that local hot spots on the catalytic surface explain the increased activity toward CH_4 conversion. The catalytic activity in SO_2 is largely maintained, as pore blockage by sulfates, as experienced in conventional heating, is counteracted.

Keywords: Perovskites; $La_{0.8}Ce_{0.2}MnO_3$; Microwave; SO_2 poisoning; Methane oxidation

1. Introduction

Whereas diesel engines have favorable engine efficiency and therefore contribute to the reduction of greenhouse gases, environmental pollution by diesel-engine exhausts in the form of soot particulate matter is of increasing concern [1–3]. Due to the carcinogenic nature of soot, soot emission standards will be tightened drastically in Europe in the coming 5 years. For this reason, substantial efforts are devoted to the development of new catalytic after-treatment processes [4]. Several techniques have been developed to deal with soot emissions, such as the use of homogenous fuel additives (passive regeneration) and the use of inert or catalytically active filters. Ciambelli et al. [5] showed that a reduction of the soot ignition temperature by about 180 K is possible using Cu/V/K/Cl/Ti-coated ceramic filters. Teraoka and co-workers [6,7] studied new catalysts for simultaneous NO_x-soot removal, in particular, spinel-type (AB_2O_4) and K_2NiF_4-type (A_2BO_4) materials. These authors found that the catalytic performance of these materials depends to a significant extent on the constituent metal, $CuFe_2O_4$ being superior in terms of selectivity to nitrogen formation, and a low selectivity to nitrous oxide.

A problem with passive regeneration using catalytically active filters is the sometimes too low diesel exhaust temperature. Active regeneration would either require raising the off-gas temperature, for instance, by a modified operation of the engine, or by heating the entire filter element to soot light-off temperatures. From an energetic point of view neither method can be considered to be elegant. An alternative is the use of microwave-assisted regeneration, allowing instantaneous and energetically efficient heating [8,9]. As dielectric heating is a bulk technique, it is faster than heating based on conduction. Moreover, yet unexplained and surprisingly high catalytic reaction rates have been reported [10–16]. The present objective is to assess the feasibility of using a microwave-sensitive catalytic material as a soot-filter coating. By periodic exposure to a dielectric field, the coating is allowed to reach soot ignition temperatures, resulting in the self-sustained carbon burn off.

Among different candidate materials, perovskite-type oxides have been reported as active catalysts in the oxidation of CO, hydrocarbons, and chlorinated hydrocarbons, as well as in automotive exhaust catalysis [17–20]. As compared to noble metals, perovskite-based catalysts pair a comparable activity to a high resistance to deactivation by hydrothermal sintering, and low cost [21]. Moreover, these oxides are high loss dielectric materials [22,23], which render them suitable for the present purpose. Perovskites can be described by the

* Corresponding author.
E-mail address: bliek@science.uva.nl (A. Bliek).

0021-9517/$ – see front matter
doi:10.1016/j.jcat.2003.09.016

general structural formula $ABO_{3\pm\delta}$, with A generally a lanthanide ion and B a transition metal ion. A and B can both be partially substituted by other ions, which leads to a wide variety of mixed oxides, $A_{1-x}A'_xB_{1-y}B'_yO_{3\pm\delta}$. δ is a measure of the number of structural and electronic defects and corresponding cation/anion vacancies due to nonstoichiometry [21]. In earlier work [24], we demonstrated that for La–Mn-based perovskites, these vacancies contribute to the catalytic activity in full oxidation.

To assess the practicality of these perovskites for the present purpose, we need to establish their sensitivity to SO_2 poisoning under the conditions relevant to automotive operations [25]. As SO_2 has a high electronic affinity, depending on the reaction temperature and composition of the perovskites, the sulfur species, SO_2, SO_3, SO_3^{2-}, SO_4^{2-}, and S^{2-}, have all been reported [25,26].

Currently, SO_2 poisoning is investigated for $La_{0.8}Ce_{0.2}MnO_3$ prepared by coprecipitation and used in CH_4 oxidation as a model reaction, in both conventional and dielectric heating experiments. The composition and surface structure of sulfur-poisoned catalysts have been studied using FTIR, XRD, XPS, TPR, and TEM.

2. Experimental

2.1. Catalyst synthesis and characterization

The perovskite-type oxide $La_{0.8}Ce_{0.2}MnO_3$ was prepared by coprecipitation, according to the method described elsewhere [18,24]. The chemical composition is assessed using inductively coupled plasma atomic emission spectroscopy (ICP-AES) on a multichannel Thermo Jarrel Ash ICAP 957 spectrometer, upgraded to ICAP 61. The specific surface area and pore volume were measured by nitrogen adsorption at 77 K on a Sorptomatic 1990 (CE Instruments) and evaluated using the BET equation. The density of the perovskite is measured by a Multivolume Pycnometer 1305 using He as filling gas. Crystallographic analysis was carried out by powder X-ray diffraction (XRD) on SR 5069 using a PW 1830 generator with $2\theta = 10$–$90°$, Cu-K_α radiation. Data with respect to chemical composition and physical properties are summarized in Table 1.

Infrared spectra were obtained on a Bio-Rad FTS 45A system equipped with a MCT detector with a resolution of 2 cm^{-1} in a range of 400 to 4000 cm^{-1}.

Table 1
The chemical composition and physical parameters of the $La_{0.8}Ce_{0.2}MnO_3$ perovskite

Parameter		Analysis method
Elemental composition (mol)	La:Ce:Mn = 0.72:0.18:1	ICP-AES
S_{BET}	43.3 $m^2\,g^{-1}$	N_2 adsorption
Pore volume	0.11 $cm^3\,g^{-1}$	N_2 adsorption
Mean pore diameter	10.1 nm	N_2 adsorption
Density	2.64 $g\,cm^{-3}$	Pycnometry
Solid composition	Perovskite + CeO_2	XRD

The core levels and valence electronic structure of the catalysts were studied using X-ray photoelectron spectroscopy (XPS) on a VG ESCAlab 210i-XL spectrometer with Mg-K_α (1253.6 eV) as the excitation source. The spectra were recorded in the fixed analyzer transmission mode with pass energy 70 eV and at pressures less than 10^{-10} mbar. The core level of La 3d, Mn 2p, S 2p, and Ce 4d species were recorded and relative intensities $I_{S\,2p}/I_{(La+Mn)}$ determined.

TEM images were obtained on a JEOL 2010 transmission electron microscope (point to point resolution of 0.23 nm and lattice image resolution of 0.14 nm) operated at 200 keV with a LaB_6 filament. All images were collected using a Gatan multiscan ccd camera (Model 791).

The catalysts were reduced in a thermogravimetric analysis (TGA) setup. About 200 mg of sample, weighted to ± 0.1 mg accuracy, was heated in the flow of a H_2/Ar mixture (v/v 2/1, SV $= 1.00 \times 10^{-2}$ $m^{-3}\,s^{-1}\,kg^{-1}$, Praxair, 99.999%). During reduction, the temperature was raised at 2.5 $K\,min^{-1}$ to 1073 K and kept there for 1 h. The composition of the exit gas stream was analyzed using mass spectrometry. The same experiments for about 15 mg of sample were also carried out in a temperature-programmed reduction setup (TPR) equipped with a thermal conductivity detector (TCD) in a flowing H_2/Ar mixture (v/v 2/1, SV $= 2 \times 10^{-2}$ $m^{-3}\,s^{-1}\,kg^{-1}$, Praxair, 99.999%). For reference, TPR patterns of pure $La_2(SO_4)_3 \cdot xH_2O$ (Aldrich, 99.9%) were obtained.

2.2. Microwave setup

The dielectric heating system used is a traveling wave once-through setup, with microwave radiation being absorbed by a water load after passing through the microwave cavity. The system consists of a microwave source (2.45 GHz, 1 kW), a circulator, a three-stub tuner section, a monomode microwave cavity TE_{100}, and a water load (Fig. 1). The reflection of the microwaves is minimized using the stub tuners. The wave-guide is formed by a rectangular copper channel (7.21 cm width × 3.605 cm height). The microwave source is protected from the reflected radiation by using a circulator. The temperature in the sample bed is assessed using an optical fiber (Luxtron). A quartz sample tube (i.d. = 18 mm), designed to accommodate the optical fiber, is placed perpendicular to the direction of propagation, allowing the sample bed to be uniformly exposed to microwave radiation. The optical fiber is calibrated using thermocouples. The amount of 3.35 g of $La_{0.8}Ce_{0.2}MnO_3$ perovskite (10 cm^3) was placed in the reactor and kept in place by a quartz grid, subsequently heated to 423 K in a He flow (GHSV $= 6 \times 10^2$ h^{-1}) with a heating rate of 5 $K\,min^{-1}$, followed by stabilization at 423 K for 1 h. The bulk temperature of the sample was monitored simultaneously with a thermocouple and an optical fiber. The lower detection limit of the optical fiber is 373 K.

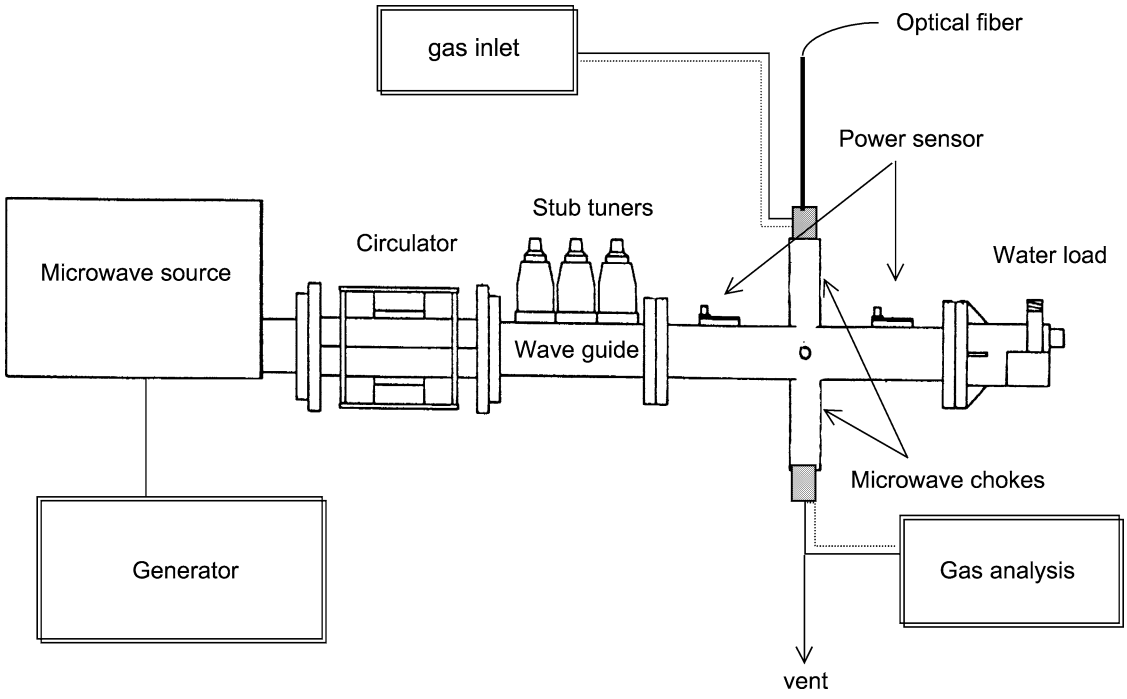

Fig. 1. Schematic drawing of 2.45 GHz microwave heating system consisting of: microwave source (Muegge, MW), generator (Muegge, MW-GIR 2M), circulator (Philips), stub tuners (Muegge), power sensor (Rhode & Schwarz), optical fiber (Luxtron, Accufiber-OFT straight end lightpipe), microwave chokes, and water load. Dashed lines denote heated tubing.

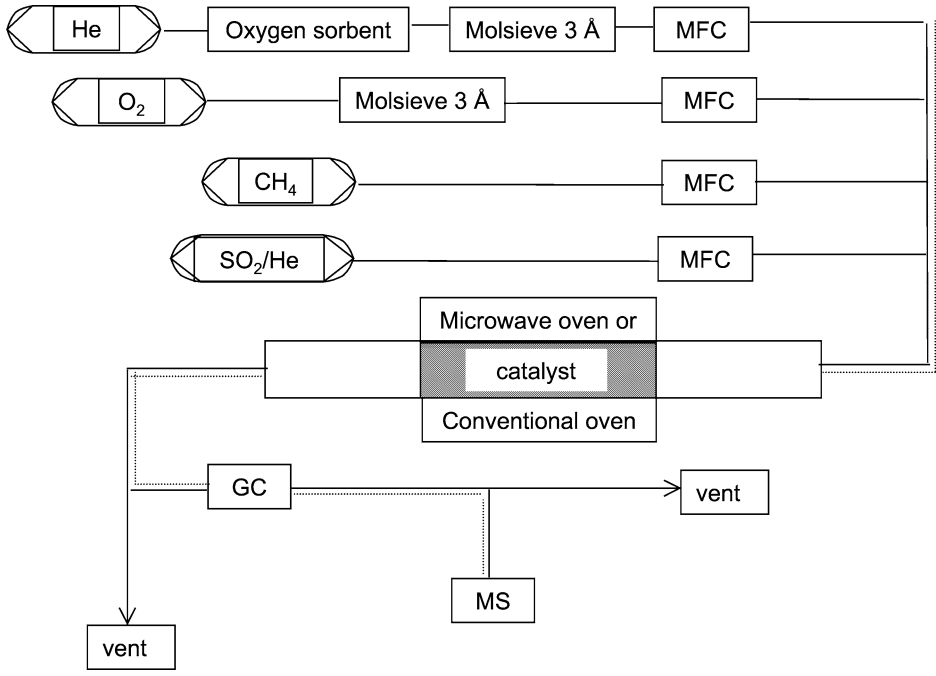

Fig. 2. Inlet manifold for the catalyzed CH_4 oxidation experiment. The quadrupole mass spectrometer (MS) and gas chromatograph are both computer controlled. The gas flow is controlled by mass flow controllers (MFC). Dashed lines denote heated tubing.

2.3. CH_4 oxidation experiments over $La_{0.8}Ce_{0.2}MnO_3$

In order to assess the catalytic activity, the oxidation of methane was used as a model reaction. It was carried out over $La_{0.8}Ce_{0.2}MnO_3$ both by dielectric and by conventional heating using a CH_4 (Praxair, 99.995%)/O_2 (Praxair, 99.5%)/He (Praxair, 99.999%) gas mixture (v/v/v 5/12.5/82.5, GHSV $= 12 \times 10^2$ h^{-1}) at a temperature of 423–723 K (Fig. 2).

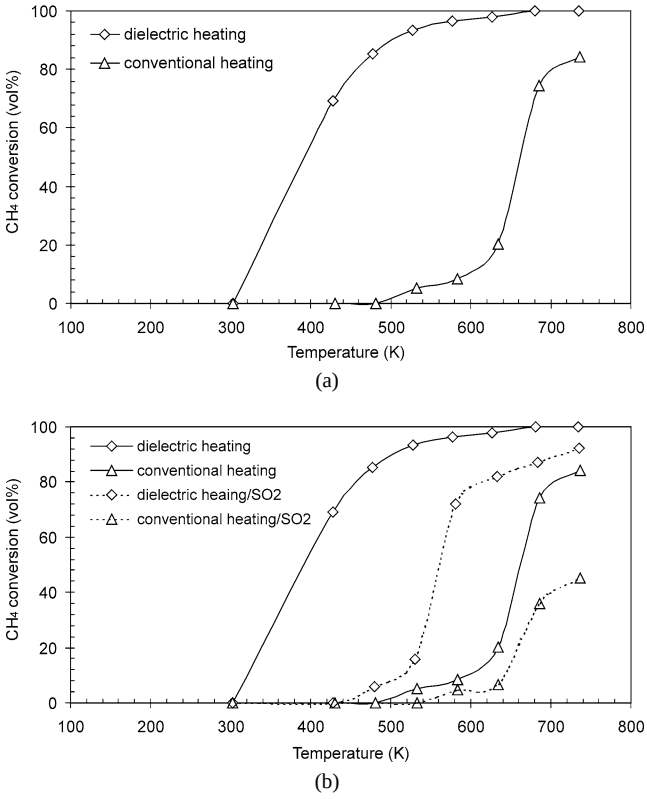

Fig. 3. CH_4 conversion versus catalyst bed temperature for dielectric and conventional experiments in the presence (a), and absence (b) of 200 ppm SO_2, GHSV $= 12 \times 10^2$ h^{-1}, $CH_4/O_2/He = 5/12.5/82.5$.

2.4. SO_2 poisoning experiments of $La_{0.8}Ce_{0.2}MnO_3$

The resistance to SO_2 poisoning was investigated by the addition of 200 ppm SO_2 (Praxair, 1007 ppm SO_2 in He) to the gas feed either at 723 K or at room temperature during temperature-programmed experiments. In both cases, the catalytic activity was assessed at 723 K. Gas composition analysis was performed using an Interscience GC equipped with four capillary columns (two Porabond Q, Molsieve plot, and Alumina), two flame ionization detectors (FID), and two thermal conductivity detectors (TCD).

3. Results

3.1. Catalytic activity of $La_{0.8}Ce_{0.2}MnO_3$ in CH_4 oxidation

$La_{0.8}Ce_{0.2}MnO_3$ activity data in CH_4 oxidation are presented in Fig. 3a, showing the conversion versus temperature for both conventional and dielectric heating. Surprisingly, the CH_4 conversion reached is substantially higher for dielectric heating.

3.2. SO_2 deactivation of $La_{0.8}Ce_{0.2}MnO_3$ in CH_4 oxidation

The influence of the presence of SO_2 on CH_4 oxidation was tested using 200 ppm SO_2 in the feed. Two types

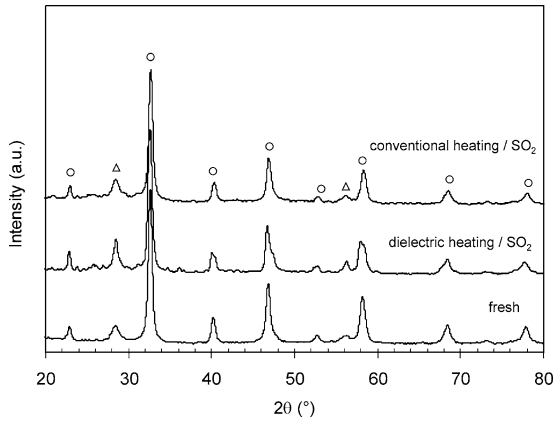

Fig. 4. XRD patterns of the fresh sample and SO_2 (200 ppm) poisoned samples during dielectric and conventional heating: perovskite (○), CeO_2 (△).

of experiments were carried out. In the first, the catalyst was brought to the reaction temperature and subsequently 200 ppm SO_2 was added to the feed stream. When the catalyst was exposed for an extended time on stream (15 h) at 723 K in the absence of SO_2, followed by 15 h at the same reaction temperature in the presence of SO_2, no significant deactivation was observed for either of the heating modes (not shown).

When SO_2 was added at 298 K, and the catalyst was subsequently subjected to a temperature-programmed experiment, a loss in activity is observed, in both conventional and dielectric heating experiments (Fig. 3b). After prolonged exposure, an irreversible deactivation is observed for conventional heating to about half of the initial activity. For dielectric heating, the activity drops only slightly to about 95% of its original level at 723 K (not shown).

The deactivation observed is accompanied by the formation of white and yellow colored separate phases. The yellow fraction was mainly observed for dielectric heating, whereas the white fraction was mostly present after conventional heating. The poisoned perovskites were analyzed by XRD, FTIR, XPS, and TEM. No significant differences between the fresh sample and the poisoned samples are detectable by XRD (Fig. 4), suggesting that the SO_2-poisoned phase exists either in amorphous form or in particle sizes below the detection limit of XRD. FTIR spectra of the catalysts deactivated by SO_2 show bands between 1000 and 1300 cm^{-1} (Fig. 5). These bands can be assigned to bulk sulfates [27,28].

The surface composition of the fresh as well as the white and the yellow fractions from the deactivated catalysts was studied by XPS. The resulting binding energy values were corrected using the C 1s peak at 285 eV. In Table 2, the corresponding binding energies of La 3d, Mn 2p, and S 2p for the fresh sample and the yellow and white fractions from the poisoned samples are listed. The binding energy of S 2p was about 169.2 eV for both fractions, which can be attributed to sulfate [26,29]. No peak was found at a binding energy of 167.3 eV, corresponding to sulfite, implying that only sulfates were formed [26,29]. The binding energy of La $3d_{5/2}$

Table 2
La 3d, Mn 2p, and S 2p binding energies for the fresh perovskite, yellow and white fraction, after SO_2 poisoning in dielectric and conventional heating

Sample	La 3d (eV)	Mn 2p (eV)	Ce 4d (eV)	S 2p (eV)	$I_S/I_{(La+Mn)}$
Fresh	834.6	642.2	121.5	–	–
	838.5	645.1	125.1		
Yellow fraction	836.0	641.4	122.0	169.2	1.5
	839.2	644.9	125.5		
White fraction	836.4	641.6	122.3	169.5	2.3
	839.6	644.7	125.7		

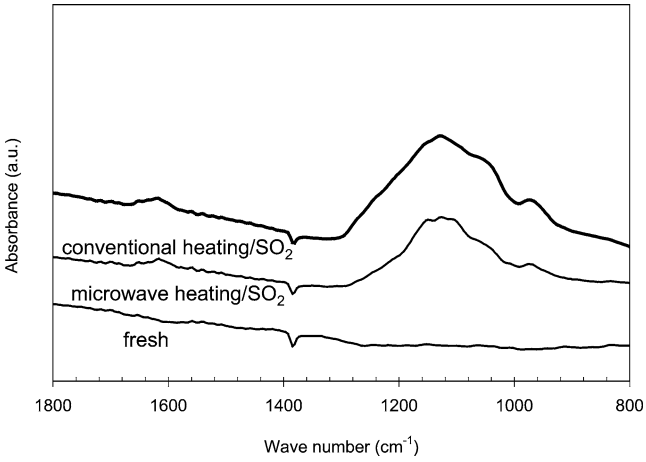

Fig. 5. FT-IR spectra of fresh sample and SO_2 (200 ppm) poisoned samples during dielectric and conventional heating.

in the fresh sample is 834.6 eV, and those of the yellow and white fraction are 836.0 and 836.4 eV, respectively (Fig. 6a). This is an indication for the formation of $La_2(SO_4)_3$ species, which has a binding energy of 836.5 eV [26,29]. The binding energy of Mn $2p_{5/2}$ in the yellow and white fraction, at 641.4 and 641.6 eV, respectively, is lower than the one in the fresh sample (642.2 eV), and similar to the binding energy of MnO. This suggests formation of a separate MnO phase from the mixed oxide. The binding energy at 122.0 eV and 125.7 eV (Fig. 6b) refers to the Ce $4d_{5/2}$ and Ce $4d_{3/2}$ components, respectively, with the spin-orbit splitting of 3.5 eV [30]. These peaks are characteristic for Ce^{4+} with a Ce $4d^9$–O $2p^6$–Ce $4f^0$ final state [30], thus indicating a cerium oxide phase. In the white fraction, however, the intensity seems to be much lower than in the fresh sample or the yellow fraction.

TEM images taken after the reaction (Fig. 7) show that sintering has occurred for the white and yellow fraction of the catalyst after CH_4 oxidation (Fig. 7b and 7c). The white fraction shows massive sintering as compared to the fresh catalyst (Fig. 7a). In contrast, in the yellow fraction, predominantly formed in the dielectrically heated sample, small particles are left on the edge of the big cluster. N_2 adsorption measurements confirm that strong sintering has occurred during conventional heating. Using BET surface area data and pore volume data the mean pore diameter after SO_2 poisoning during dielectric heating is assessed to be about 6.5 nm, and for conventional heating it is about 3.5 nm. This sintering may reduce the accessibility of the active sites.

The phases formed during deactivation were more closely investigated by TPR (Fig. 8). TPR data of the SO_2-poisoned

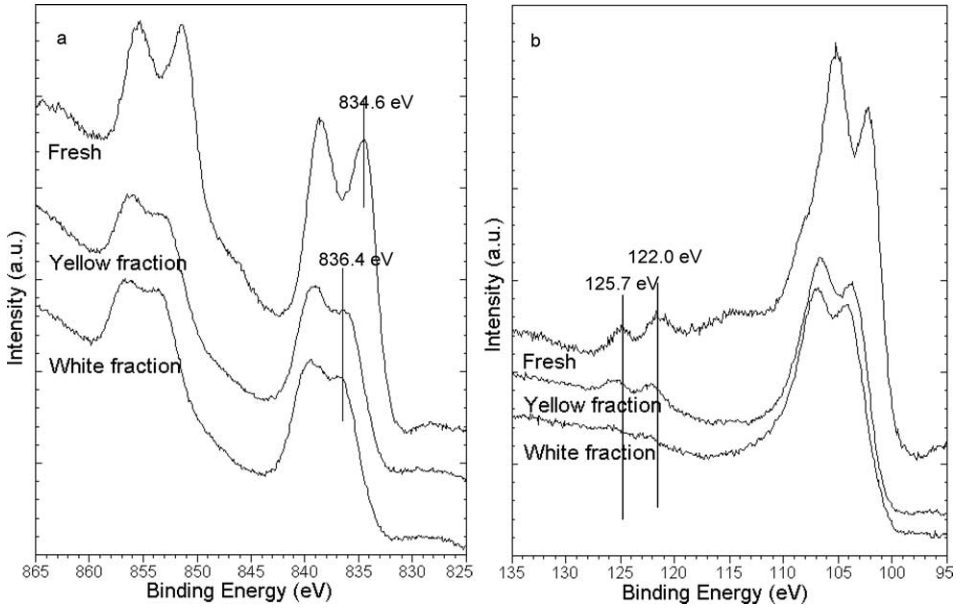

Fig. 6. XPS La 3d (a) and Ce 4d (b) spectra for the fresh catalyst, and the yellow and white fractions obtained after SO_2 poisoning.

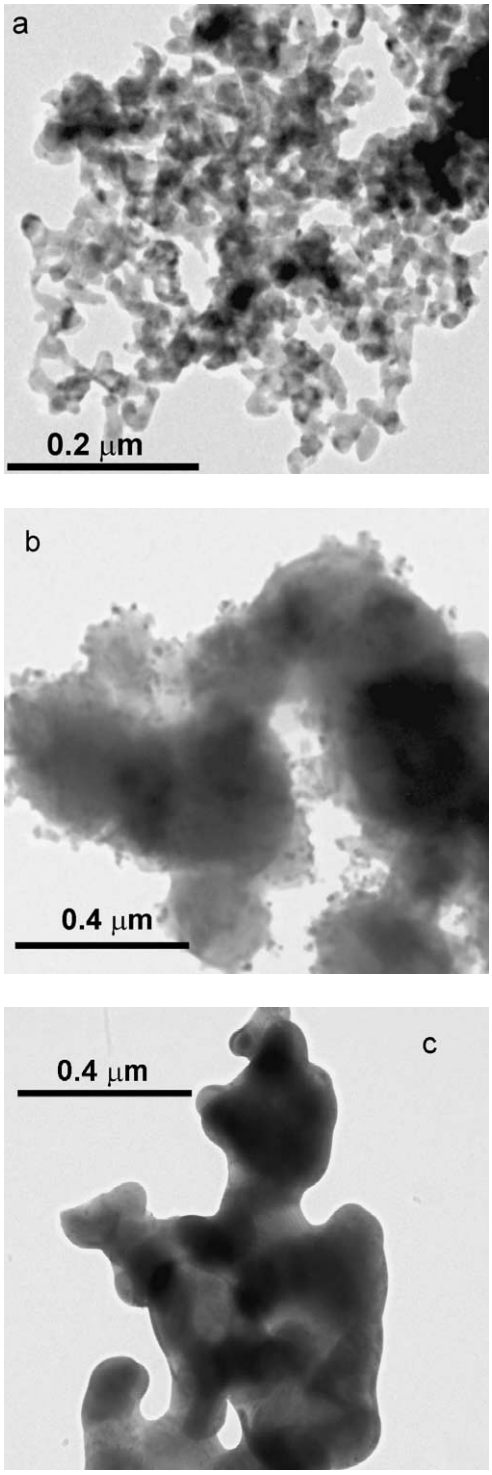

Fig. 7. TEM image of fresh $La_{0.8}Ce_{0.2}MnO_3$ sample (a), the yellow fraction, and (b) the white fraction (c).

catalyst during conventional heating show a similar profile as pure $La_2(SO_4)_3 \cdot xH_2O$. Reduction takes place in two steps with peaks at 862 and 966 K. In contrast, the catalyst deactivated in a dielectric field shows a broad reduction band. After a H_2 treatment in the TGA, XRD patterns have been recorded for the fresh sample and the poisoned ones in

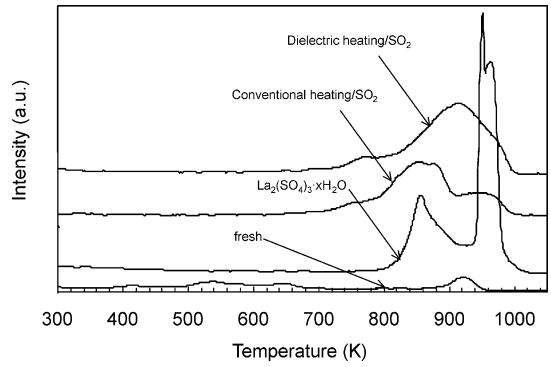

Fig. 8. TPR patterns of fresh and spent SO_2-poisoned samples after dielectric and conventional heating, as well as of pure lanthanum sulfate. The temperature was raised with 5 K min^{-1} to 1073 K and maintained at 1073 K for 1 h (v/v 2/1, SV = 2×10^{-2} m^{-3} s^{-1} kg^{-1}).

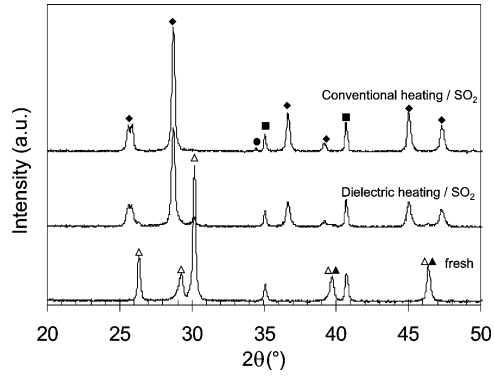

Fig. 9. XRD patterns after H_2 reduction of the fresh catalyst, SO_2 poisoned during dielectric and conventional heating: La_2O_3 (△), MnO (■), Ce_2O_3 (▲), La_2O_2S (◆), Ce_2S_3 (●).

both the dielectric and the conventional oven (Fig. 9). The samples have become gray/green after reduction at 1073 K, suggesting the formation of new phases. The XRD pattern reveals the disappearance of the perovskite phase, with concurrent formation of individual La_2O_3, MnO, and Ce_2O_3 for the fresh sample. The XRD data obtained from both deactivated catalysts shows a strong characteristic peak of lanthanide oxide sulfide (La_2O_2S), formed by reduction of lanthanum sulfate. No evidence was found for the formation of $MnSO_4$ in the presence of SO_2. A small amount of Ce_2S_3 was observed after the reduction treatment for the poisoned sample only when conventional heating was used.

4. Discussion

4.1. Catalytic performance in conventional and dielectric heating

The catalytic activity in CH_4 full oxidation is considerably higher during dielectric heating than during conventional heating. It has been postulated that dielectric heating may result in selective heating of catalytic sites with respect to their direct surroundings, thus leading to “molecular hot

spots" [31]. When a material contains strongly absorbing active sites such as dipoles, microwave energy will be absorbed selectively by active sites and these so-called hot spots will be generated. The A and B sites of perovskite-type oxides have been shown to have different dipole strengths [32]. Therefore, hot spot formation is possible for perovskites during dielectric heating. Reactant molecules adsorbed on such a hot active site may be activated by subsequent energy transfer from the site to the adsorbed molecule. The difference between local temperature of the hot spots and the bulk mean temperature can be up to several hundred of degrees [33]. Generation of hot spots is of great importance in heterogeneous catalysis because reactions on active sites may take place at much higher temperatures than at the measured bulk temperature of the catalyst. Therefore, the reaction rate can be much higher than under conventional heating.

An additional conventional explanation for the observed high reaction rate may simply be that due to the bulk heating nature of dielectric heating, the intraparticle temperature may be substantially higher than the surface temperature during dielectric heating, for similar surface temperatures.

4.2. Deactivation by SO_2

A loss in catalytic activity in the presence of SO_2 is observed for both heating modes at low temperatures. This may be due to the competitive adsorption between gas-phase oxygen and SO_2 followed by sulfate formation, since methane oxidation at low temperature is a suprafacial reaction involving oxygen coming from gas phase or sitting at the oxygen vacancies of the catalysts [34]. The superior catalytic performance for dielectric heating in the presence of SO_2 introduced in the gas feed at 298 K is in line with the results from Turner et al. [35] for a commercial Pt–Rh-based three-way automotive catalyst. These authors observed an improved performance in SO_2-containing exhaust gases for combined dielectric/conventional heating, as compared to conventional heating only. This result was attributed to selective absorption of microwave radiation by sulfides and sulfates, with subsequent decomposition into SO_2.

Our results indicate that neither for dielectric heating nor for conventional heating a significant loss in catalytic activity occurs when SO_2 is added at 723 K. Alifanti et al. [36] observed that $La_{0.9}Ce_{0.1}CoO_3$, $La_{0.8}Ce_{0.2}CoO_3$, and $La_{0.8}Ce_{0.2}MnO_3$ compositions are least sensitive to SO_2 poisoning from the series of $La_{1-x}Ce_xMn_{1-y}Co_yO_3$ perovskites ($x = 0$, 0.1, 0.2, 0.3 and $y = 0.5$, 0.6, 0.7) at 823 K. Following a 15-h period of exposure at 823 K to 20 ppm SO_2 added to the feed, the activity in methane oxidation was shown to remain at a stable level in excess of 80% of the original value. Our deactivation data—indicating that deactivation is limited when SO_2 is added at high temperature—strongly suggest that this is the result of weak adsorption of SO_2 at these temperatures, which additionally arises from the competitive adsorption of H_2O produced in the oxidation reaction (not shown).

After prolonged exposure of the catalysts to SO_2 at 298 K, and the subsequent temperature-programmed reaction, formation of bulk sulfates was observed by FTIR measurements. The surface electron structure recorded by XPS of the white and yellow fractions obtained after SO_2 poisoning shows that $La_{0.8}Ce_{0.2}MnO_3$ is deactivated predominantly by irreversible formation of lanthanum sulfate. This is confirmed by the XRD patterns of the reduced poisoned samples, which indicate a strong characteristic peak of lanthanide oxide sulfide formed during the reduction of the sulfate. Formation of MnO is observed by XPS and XRD, while no evidence is found for the formation of Mn sulfates. Finally, XPS data show a decrease in the Ce 4d peak intensity for the white fraction, indicating that the original Ce oxidic structure has been destroyed, most likely due to the formation of cerium sulfate. This is also confirmed by XRD data after reduction: a characteristic peak of Ce_2S_3 is observed for the reduced poisoned sample when conventional heating is used.

Since the poisoned sample using dielectric heating mainly contains the yellow fraction, poisoning in the microwave mainly affects the La cation by formation of $La_2(SO_4)_3$. For conventional heating, SO_2 poisoning affects both La and Ce cations by formation of sulfates, as indicated by the predominant presence of the white fraction. The $I_S/I_{(La+Mn)}$ ratio, as determined by XPS (Table 2), shows that the white fraction contains 50% more sulfate species than the yellow fraction. The formation of cerium sulfates can be considered indicative of the destruction of the anion vacancies, which are responsible for the catalytic activity.

4.3. SO_2-poisoning mechanism over $La_{0.8}Ce_{0.2}MnO_3$

During both dielectric and conventional heating, the presence of SO_2 leads to an irreversible formation of lanthanum sulfate and thus to deactivation of the catalyst. It is known that the concentration of sulfates increases with rising reaction temperature, as the formation of sulfates is controlled by the reaction kinetics [29]. During conventional heating (based on thermal conduction), the exterior of the particles is highest in temperature and the formation rate of formed lanthanum sulfates is thus highest in this region. Therefore, deactivation predominantly takes place at the exterior of the particles through a shell-progressive mechanism (Fig. 10a). The formation of sulfates is accompanied by pore blockage, as indicated by TEM and BET data. This deactivation process thus results in limitation of the access to the catalytic surface. In contrast, the interior of the catalytic particle is highest in the temperature during dielectric heating, based on its bulk heating nature, by creating an effectively *inverse* temperature gradient throughout the catalytic particle. For this reason, deactivation by formation of sulfates occurs predominantly in the interior of the catalytic particles as a result of the high temperature in the interior of the par-

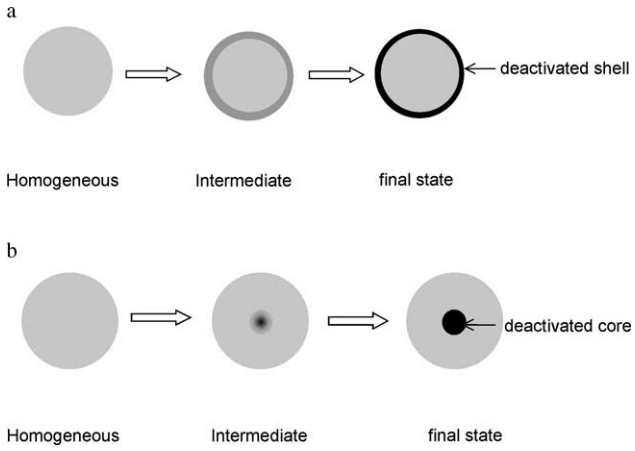

Fig. 10. SO_2-poisoning mechanism over $La_{0.8}Ce_{0.2}MnO_3$ perovskite during conventional heating through shell progressive (a) and dielectric heating through growing core (b).

ticles. Thus, deactivation during dielectric heating proceeds through a growing core mechanism, as shown in Fig. 10b. Moreover, the temperature gradient persists for both heating modes, even in steady state, due to the exothermic nature of the reaction. Whereas the activity is thus lost by lanthanum sulfate formation, the impact of pore blockage is only limited. The exterior of particles is still accessible to reactants and deactivation is slower than during conventional heating. This seems to be confirmed by TPR data: the broad reduction peak found over a temperature range of 200 K for dielectrically heated sample is likely to be the result of (slow) diffusion of H_2 into the center of the catalyst particle, which subsequently reduces the formed sulfate.

5. Conclusion

The high catalytic activity toward CH_4 oxidation over $La_{0.8}Ce_{0.2}MnO_3$ perovskites observed during dielectric heating, as compared to conventional heating, can be explained by the higher particle center temperature, which in turn is the result of the bulk heating nature of dielectric heating. Deactivation of these perovskites by SO_2 is comparatively slow at high temperatures, as a result of weak adsorption of SO_2. Irreversible loss in activity occurs after prolonged exposure of the catalyst to SO_2 due to the formation of lanthanum sulfate. Cerium sulfate is formed predominantly during conventional heating, which contributes to deactivation by elimination of anion vacancies that are responsible for the catalytic activity. Deactivation is faster for conventional heating than for dielectric heating. This is to be attributed to the concerted effort of lanthanum sulfate formation and the resulting pore blockage, which limits the accessibility toward the reactants. As during conventional heating pore blockage occurs mainly at the outer core, the result is a fast, shell-progressive deactivation. In contrast, when sulfate formation mainly occurs in the particle interior (through a growing core mechanism), as is the case during dielectric heating, deactivation is less fast.

Acknowledgments

The financial support of Netherlands Research Council for this project is gratefully acknowledged. Thanks are due to Mr. R. Haswell and Mr. G. Jonkers from Shell Research & Technology Centre Amsterdam for performing TEM and XPS, to Mr. T. Visser and F. Soulimani from the University of Utrecht and Mr. L.M. van der Zande from the University of Amsterdam for FT-IR, to Mr. J. Elgersma for ICP, and Mrs. M.C. Mittelmeijer-Hazeleger for N_2 adsorption measurements.

References

[1] S. Ponce, M.A. Peña, J.L.G. Fierro, Appl. Catal. B 24 (2000) 193.
[2] S.S. Hong, G.D. Lee, Catal. Today 63 (2000) 397.
[3] Y. Teraoka, K. Kanada, S. Kagawa, Appl. Catal. B 34 (2001) 73.
[4] P. Zelenka, W. Cartellieri, P. Herzog, Appl. Catal. B 10 (1996) 3.
[5] P. Ciambelli, V. Palma, P. Russo, S. Vaccaro, Ind. Eng. Chem. Res. 39 (2000) 4914.
[6] W.F. Shangguan, Y. Teraoka, S. Kagawa, Appl. Catal. B 8 (1996) 217.
[7] Y. Teraoka, K. Nakano, W. Shangguan, S. Kagawa, Catal. Today 27 (1996) 107.
[8] J.X. Ma, M. Fang, P. Li, B. Zhu, X.H. Lu, N.T. Lau, Appl. Catal. A 159 (1997) 211.
[9] J.W. Tang, T. Zhang, L. Ma, N. Li, D.B. Liang, L.W. Lin, J. Catal. 211 (2002) 560.
[10] P. Lidström, J. Tierney, B. Wathey, J. Westman, Tetrahedron 57 (2001) 9225.
[11] J.W. Tang, T. Zhang, D.B. Liang, H.H. Yang, N. Li, L.W. Lin, Appl. Catal. B 36 (2002) 1.
[12] N. Kuhnert, Angew. Chem., Int. Ed. Engl. 41 (2002) 1863.
[13] A. Stadler, S. Pichler, G. Horeis, C.O. Kappe, Tetrahedron 58 (2002) 3177.
[14] R. Pérez, T. Beryozkina, O.I. Zbruyev, W. Haas, C.O. Kappe, J. Comb. Chem. 4 (2002) 501.
[15] G.A. Strohmeier, C.O. Kappe, J. Comb. Chem. 4 (2002) 154.
[16] E. Van der Eycken, P. Appukkuttan, W. De Borggraeve, W. Dehaen, D. Dallinger, C.O. Kappe, J. Org. Chem. 67 (2002) 7904.
[17] K.S. Song, H.X. Cui, S.D. Kim, S.K. Kang, Catal. Today 47 (1999) 155.
[18] D. Kießling, R. Schneider, P. Kraak, M. Haftendorn, G. Wendt, Appl. Catal. B 19 (1998) 143.
[19] H.M. Zhang, Y. Shimzu, Y. Teraoka, N. Miura, N. Yamazoe, J. Catal. 121 (1990) 432.
[20] R.J.H. Voorhoeve, D.W. Johnson Jr., J.P. Remeika, P.K. Gallagher, Science 195 (1977) 827.
[21] L. Forni, I. Rossetti, Appl. Catal. B 38 (2002) 29.
[22] T.A. Vanderah, C.K. Lowe-Ma, D.R. Gagnon, J. Am. Ceram. Soc. 77 (1994) 3125.
[23] B. Vaidhyanathan, D.K. Agrawal, T.R. Shrout, Y. Fang, Mater. Lett. 42 (2000) 207.
[24] Y. Zhang-Steenwinkel, J. Beckers, A. Bliek, Appl. Catal. A 235 (2002) 79.
[25] L. Wan, in: L.G. Tejuca, J.L.G. Fierro (Eds.), Properties and Applications of Perovskite-Type Oxides, Dekker, New York, 1993, p. 145.
[26] Y.F. Zhu, R.Q. Tan, J. Feng, S.S. Ji, L.L. Cao, Appl. Catal. A 209 (2001) 71.

[27] S. Hodjati, C. Petit, V. Pitchon, A. Kiennemann, Appl. Catal. B 30 (2001) 247.
[28] I. Rosso, E. Garrone, F. Geobaldo, B. Onida, G. Saracco, V. Specchia, Appl. Catal. B 30 (2001) 61.
[29] H. Wang, Y.F. Zhau, R.Q. Tan, W.Q. Yao, Catal. Lett. 82 (2002) 199.
[30] D.R. Mullins, S.H. Overbury, D.R. Huntely, Surface Sci. 409 (1998) 307.
[31] L. Seyfried, F. Gairn, G. Maire, J.M. Thiébaut, G. Roussy, J. Catal. 148 (1994) 281.
[32] N. Setter, E. Colla, I. Reaney, R. Zurmuehlen, D. Dube, J. Petzelt, Ferroelectrics 154 (1994) 231.
[33] M. Hájek, in: A. Breccia, A.C. Metaxas (Eds.), Microwave and High Frequency Heating Principles and Chemical Application, Unità Complessa di Scienze Chimiche, Università di Bologna, Italy, 1997, p. 85.
[34] M.A. Peña, J.L.G. Fierro, Chem. Rev. 101 (2001) 1981.
[35] M.D. Turner, R.L. Laurence, K.S. Yngvesson, W.C. Conner, Catal. Lett. 71 (2001) 133.
[36] M. Alifanti, A. Auer, J. Kirchnerova, F. Thyrion, P. Grange, B. Delmon, Appl. Catal. B 41 (2003) 71.